Low-Frequency Pycnocline Depth Variability at Ocean Weather Station P in the Northeast Pacific

PATRICK F. CUMMINS

Institute of Ocean Sciences, Sidney, British Columbia, Canada

GARY S. E. LAGERLOEF

Earth and Space Research, Seattle, Washington

(Manuscript received 5 September 2001, in final form 3 May 2002)

ABSTRACT

Low-frequency variability of the depth of the main pycnocline at Ocean Weather Station P and over the northeast Pacific is examined in terms of the one-dimensional response to local Ekman pumping according to the Hasselmann stochastic climate model. The model is forced with monthly wind stress curl anomalies derived from the National Centers for Environmental Prediction reanalysis for the period 1948–2000. An empirical orthogonal function analysis shows that the leading mode of the response bears the signature of the Pacific (inter) Decadal Oscillation (PDO) and that the associated principal component captures the ''regime shift'' of 1976/77. The correlation is 0.77 between annually averaged pycnocline displacement anomalies hindcast from the model and anomalies in the depth of the main pycnocline at station P (50°N, 215°E) observed over a 43-yr period. The comparison indicates that variability in the depth of the upper layer on interannual to interdecadal timescales at station P occurs largely as an integrated response to local Ekman pumping. In addition, the results suggest that the PDO mode dominates the observed variability.

1. Introduction

The occurence of low-frequency, upper-ocean thermal variability in the North Pacific is well documented. Anomalies in sea surface temperature (SST), subsurface thermal structure, and upper-ocean heat content are known to display significant variability at interannual to interdecadal timescales (e.g., Deser et al. 1996; Zhang et al. 1997; White and Cayan 1998; Tourre et al. 1999).

The Pacific (inter) Decadal Oscillation (PDO) is a mode of low-frequency variability that is expressed in several atmospheric and oceanic fields (Mantua et al. 1997). It is represented typically in terms of the leading mode in an empirical orthogonal function (EOF) analysis of SST over the extratropical North Pacific. The canonical spatial pattern of the PDO consists of a horseshoe-shaped region, including the Gulf of Alaska and eastern Pacific waters, that varies in opposition to the central Pacific region. Long-lived changes in the polarity of the PDO have been termed ''regime shifts'' (Mantua et al. 1997). One such transition occurred in 1976/77, as the mode reversed polarity from a cold to a warm phase, associated with warmer SST and upper-ocean temperatures in the Gulf of Alaska and along the west coast of North America. As an EOF mode, the PDO encompasses variability over a range of timescales from interannual to interdecadal. Tourre et al. (2001) presented a joint frequency domain analysis of SST and sea level pressure variability over the Pacific from 30°S to 60°N. Distinct patterns of coherent decadal and interdecadal variability were found, with the regime transition of 1976/77 identified as part of the interdecadal signal.

While upper-ocean temperature variability is reasonably well described by the existing database, low-frequency variations in the mass field of the upper ocean are less well defined. Salinity is an important factor determining the potential density distribution, especially in the subarctic Pacific. The relative paucity of salinity data thus presents a significant constraint for hindcast studies (Overland et al. 1999). To overcome the limitation, Lagerloef (1995) combined available temperature and salinity measurements with historical *T*–*S* relations to construct 0–450-dbar dynamic height fields over the Gulf of Alaska (50°–60°N, 200°–230°E) for the period 1968–90. The results show variability on interdecadal timescales, with a transition from negative to positive anomalies occurring at large scales over the region in the late 1970s. Freeland et al. (1997) discuss variations in the depth of the main pycnocline at Ocean Weather Station P (50°N, 215°E), one of the few locations with a relatively long time series of subsurface temperature

Corresponding author address: Patrick F. Cummins, Institute of Ocean Sciences, P.O. Box 6000, 9860 W. Saanich Rd., Sidney, BC V8L 4B2, Canada.
E-mail: cumminsp@dfo-mpo.gc.ca

and salinity. Low-frequency variability is evident in the record; a trend is also identified with the depth of the main pycnocline apparently shoaling at a rate of approximately half a meter per year since 1957.

A considerable modeling effort has been devoted to identifying the mechanisms of low-frequency variability in the North Pacific. Coupled models show generic PDO-like variability arising through coupled atmosphere–ocean interactions (e.g., Latif and Barnett 1994; see Miller and Schneider 2000 for a review). Time-dependent simulations of the 1976/77 regime shift were presented by Miller et al. (1994, 1998). These studies employed a sophisticated ocean circulation model forced with time-dependent wind stress and surface heat flux anomalies for the period 1970–88. The authors were able to simulate the observed regime shift in SST (Miller et al. 1994) and temperature at depth 400 m (Miller et al. 1998). Results from the latter suggested that thermocline variability east of the date line was driven by the curl of the wind stress, with Sverdrup dynamics dominating the vorticity balance. On the other hand, Lagerloef (1995) applied a local stochastic climate model (Hasselmann 1976; Frankignoul and Hasselmann 1977) and showed through canonical correlation analysis that time-dependent Ekman pumping dynamics could account for low frequency dynamic height variability over the Gulf of Alaska.

In this paper we extend the work of Lagerloef (1995) and examine the response of the local stochastic climate model to Ekman pumping over the northeast Pacific (30°–60°N, 180°–240°E). The model is driven by forcing fields derived from the National Centers for Environmental Prediction (NCEP) reanalysis and used to construct pycnocline depth variations for the period 1948–2000. In particular, we examine the ability of this simple model to hindcast pycnocline depth anomalies at station P. A direct comparison with observations is made to assess the extent that the observed low frequency variability may be attributable to local Ekman pumping. To set the results within a larger-scale context, we show that the model response supports an analog to the PDO and consider the influence of this mode at station P.

In the next section, the model and forcing fields are discussed. This is followed by an examination of the leading mode of variability of the model response over the northeast Pacific. In section 3, the results are compared with observations drawn from Freeland et al. (1997). Conclusions are given in section 4.

2. Stochastic climate model

The stochastic climate model advanced by Hasselmann (1976) is applied to examine the response to Ekman pumping at station P and over the northeast Pacific. In this model, low-frequency climatic variability arises as the ocean integrates the local transient atmospheric weather forcing, which typically has a white frequency spectrum. The role of ocean dynamics in the model is essentially a dissipative one, serving to limit the response to the forcing. A scale separation is postulated between the short decorrelation timescale of the atmospheric forcing and the longer timescales associated with internal dissipation of oceanic fluctuations.

Generalizations to this approach have been developed that allow for the presence of baroclinic Rossby waves (e.g., Müller and Frankignoul 1981). In particular, Frankignoul et al. (1997) advanced a quasigeostrophic model for decadal variability consisting of the local wind-forced response and long Rossby waves generated in the presence of an eastern boundary. Qui (2002) applied this model to hindcast areal averages of sea surface height anomalies measured by satellite altimetry over the North Pacific. In the present study, consideration is given to the local model, which we show to be sufficient for modeling the pycnocline depth variability observed at station P. Application of a more complete quasigeostrophic model will form the subject of a future study.

Pycnocline depth variability is then assumed to be governed by a simple Markovian model of local Ekman pumping (Frankignoul and Hasselmann 1977; Lagerloef 1995),

$$\frac{dh}{dt} = w_e - \lambda h, \tag{1}$$

where h represents the isopycnal displacement anomaly (positive upward) and w_e is the Ekman pumping velocity. The decay parameter, $\lambda > 0$, specifies the timescale (λ^{-1}) over which fluctuations in h are damped. The Rayleigh damping term in (1) amounts to a parameterization of internal ocean dynamics as a negative feedback on the system. This encompasses terms from more complete equations that would incorporate detailed mixing and entrainment processes and turbulent transfers (Lagerloef et al. 1998). As such, a simple closure is posited for these unresolved and complex processes as a linear stabilizing feedback. With $\lambda = 0$, (1) reduces to a passive oceanic response to atmospheric forcing with the influence of internal ocean dynamics omitted entirely.

The Ekman pumping velocity w_e is related to the wind stress $\boldsymbol{\tau}$ as

$$w_e = \hat{\mathbf{z}} \cdot \boldsymbol{\nabla} \times \frac{\boldsymbol{\tau}}{\rho f} = (\rho f)^{-1}\left[\hat{\mathbf{z}} \cdot \boldsymbol{\nabla} \times \boldsymbol{\tau} + \frac{\beta \tau^x}{f}\right], \tag{2}$$

where ρ is a constant reference density, $f = 2\Omega \sin\theta$ is the Coriolis parameter with θ the latitude and Ω the rotation rate of the earth, τ^x is the zonal component of the wind stress, and $\beta = 2\Omega \cos\theta / R_e$ with R_e the radius of the earth. The first term in brackets is the vertical component of the curl of the wind stress. The second term, arising from differentiation of the Coriolis parameter, is a minor correction to the first. We have verified that omitting this term leaves results virtually unchanged.

The transfer function associated with (1) is $T(\omega) = (\omega^2 + \lambda^2)^{-1}$ with ω the angular frequency. Thus the ocean acts as a low-pass filter, producing a red noise spectrum given white noise atmospheric forcing. There is a phase lag between the response and the forcing, $\phi = \tan^{-1}(\omega/\lambda)$, that varies from $\phi = 90°$, as $\omega/\lambda \to \infty$, to $\phi = 0°$, as $\omega/\lambda \to 0$ (Lagerloef 1995).

Writing $t = n\Delta t$, (1) is discretized according to a second-order accurate trapezoidal scheme as

$$h^{n+1} = \alpha_1 h^n + \alpha_2 w_e^{n+1/2}, \tag{3}$$

where $\alpha_1 = (2 - \lambda\Delta t)/(2 + \lambda\Delta t)$ and $\alpha_2 = 2\Delta t/(2 + \lambda\Delta t)$. Equation (3) has the form of a first-order autoregressive process with the ''memory'' of the system determined by the timescale, λ^{-1}. If w_e is assumed to be uncorrelated noise, then α_1 may be identified as the value of the autocorrelation function at unit lag (von Storch and Zwiers 1999), thus providing an empirical means of estimating $\lambda^{-1} = 0.5\Delta t\ (1 + \alpha_1)/(1 - \alpha_1)$. The initial condition is taken arbitrarily as $h(t = 0) = 0$ and has no further effect on the solution after a few decay timescales have elapsed.

For simplicity, a spatially uniform value for λ^{-1} is considered. In a linear fit to dynamic height anomalies in the Gulf of Alaska, Lagerloef (1995) found the appropriate damping timescale varied between 0.5 and 2.5 yr, with a median value of about 1 yr. As noted above, the autocorrelation function may also be used to estimate λ from observations. For example, the PDO index may be regarded as representative of extratropical, upper-ocean variability over the North Pacific. Here the PDO index is defined as the leading principal component of SST variability over the extratropical North Pacific (Mantua et al. 1997). At unit lag, the autocorrelation of annual mean values of the PDO index over the period 1900–2000 is 0.53, yielding $\lambda^{-1} = 1.6$ yr. Using the index over only the shorter period of 1948–2000 gives a slightly longer timescale of 2 yr. By comparison, the record of yearly pycnocline depth anomalies at station P considered in section 3 (with short gaps filled by linear interpolation) yields $\lambda^{-1} = 1.4$ yr. In the following, we take the reference value of λ^{-1} as 1.5 yr and examine the sensitivity of the response to variations in the parameter.

a. Ekman pumping velocity

Monthly fields of Ekman pumping velocity for the period 1948–2000 were derived from monthly mean wind stresses available at a resolution of 1.875° lon × 1.904° lat from the NCEP reanalysis. The resulting fields were linearly interpolated to a uniform 1° × 1° grid. Aside from peaks at the annual frequency and its semiannual harmonic, spectra of the Ekman pumping velocity (not shown) north of 30°N are nearly white for periods longer than about 100 days. The white noise level generally increases to the north over the North Pacific, a tendency also noted by Chave et al. (1991) with respect to wind stress curl spectra. However, the latitudinal dependence is weaker in Ekman pumping velocity spectra because of the compensating f^{-1} factor appearing in (2).

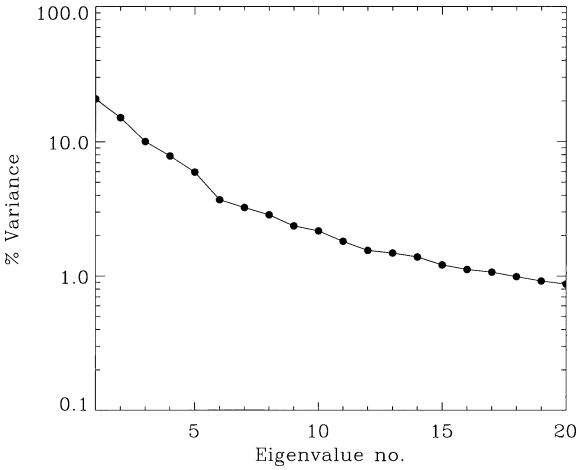

FIG. 1. The normalized spectrum of eigenvalues from an EOF analysis of Ekman pumping velocity derived from the NCEP reanalysis monthly mean stresses. The first (1, 5, 10, 20) modes account for (21%, 60%, 74%, 86%) of the total variance, respectively.

It is useful to expand the Ekman pumping velocity in (1) as a truncated sum of empirical orthogonal modes,

$$w_e = \sum_{m=1}^{M} F_m(\mathbf{x}) a_m(t), \tag{4}$$

where $F_m(\mathbf{x})$ denotes the spatial pattern (EOF) of mode m and a_m is the associated principal component (PC). We consider the response to the first M modes, effectively filtering the forcing data to retain only the most significant and meaningful variability. Spurious or erroneous signals are most likely associated with the smallest spatial scales contained in the higher modes.

Figure 1 shows the spectrum of eigenvalues resulting from an EOF expansion of the Ekman pumping velocity derived from the NCEP reanalysis. A change in the slope of the eigenspectrum occurs between modes 5 and 6. Application of the sampling criteria of North et al. (1982) suggests that modes higher than mode 6 are not well separated. Nevertheless, these higher modes may represent meaningful variability, and an optimal choice for the number of forcing modes is uncertain.[1] Accordingly, we have treated the truncation limit, M, as a parameter and considered the sensitivity to variations about the reference value of $M = 5$. As noted below, the results are relatively insensitive to the inclusion of additional higher modes in the forcing.

The spatial patterns of the first and second EOFs and

[1] Application of rule N, a selection rule based on a Monte Carlo method (Preisendorfer 1988), would indicate that approximately 32 modes are statistically different than ''noise.'' However, the usefulness of selection rules is disputed (von Storch and Zwiers 1999) and no significance is attached here to this result.

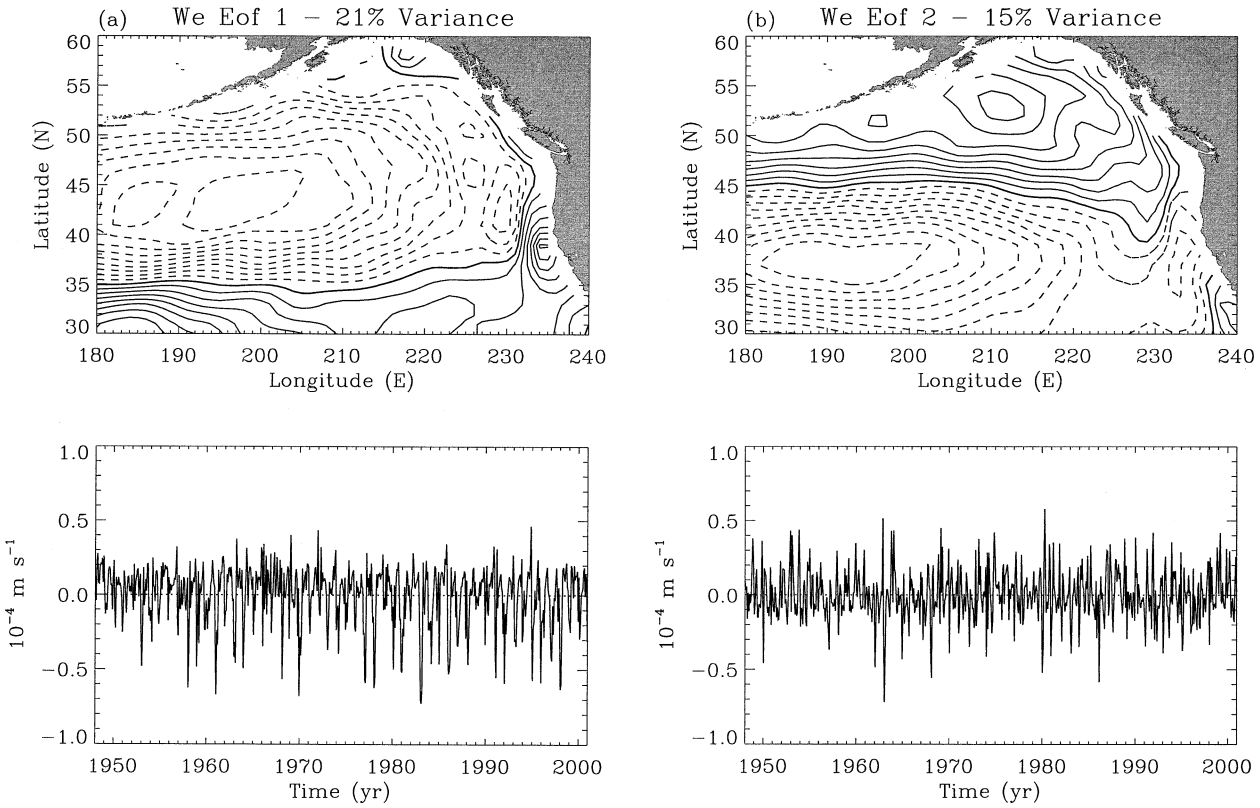

FIG. 2. The (a) first and (b) second EOFs and PCs of the Ekman pumping velocity over the northeast Pacific. The EOFs were determined using the covariance method and have been normalized to have a maximum absolute value of 1. The contour interval is 0.1; dashed contours indicate negative values.

PCs of the Ekman pumping velocity (Figs. 2a and 2b) bear some similarity to the leading wind stress curl EOFs given in Reinecker and Ehret (1988). The first Ekman pumping mode (Fig. 2a) is associated with fluctuations in the intensity of the Aleutian low pressure system, while the second (Fig. 2b) reflects north–south oscillations between the Aleutian low and the subtropical high.

The PCs of Fig. 2 are noisy, reflecting short-timescale weather fluctuations and the modulation of these fluctuations over longer periods. The PC of the first mode is highly correlated with the North Pacific (NP) index developed by Trenberth and Hurrell (1994) to characterize atmospheric variability over the North Pacific. The NP index is a time series of area-weighted, monthly mean sea level pressure anomalies over the region 30°–65°N, 160°–220°E. Figure 3 shows a low-pass filtered version of the NP index together with a similarly filtered version of the leading PC of the Ekman pumping velocity. Note that filtering reduces the variability considerably; in comparison with Fig. 2, the scale of the vertical axes is smaller by a factor of 100. A weak long-term trend is apparent in Fig. 3 such that anomalies are predominantly positive (negative) for the period before (after) the mid-1970s. These changes are associated with eastward displacement and deepening of the mean wintertime Aleutian low following the winter of 1976/77 (Trenberth and Hurrell 1994). Similar trends occur in the PCs of higher modes, although they are not as readily apparent as in the gravest mode.

b. Response over the northeast Pacific

Monthly pycnocline depth anomaly fields were synthesized from (3) with the forcing given according to (4). An EOF analysis was then applied to determine the dominant mode of variability produced by the model. Figure 4 gives the resulting leading EOF and PC of h (henceforth EOF1 and PC1, respectively) from the reference case. EOF1 shows an extensive region over the central Pacific, centered near 47°N, 205°E, varying in opposition with the northern Gulf of Alaska and a band adjacent to the North American coast. PC1 shows low-frequency variations over a range of ± 25 m with generally positive anomalies prior to 1977 and negative anomalies afterward. Combined with EOF1, this implies interdecadal variability with shoaling of the pycnocline over the central Pacific after 1977. There is a concommitent deepening in the Gulf of Alaska and over a region in proximity to the North American continent. The ''regime shift'' appears as a rather abrupt transition in the sign of PC1 in 1977. The results of Fig. 4 remain largely

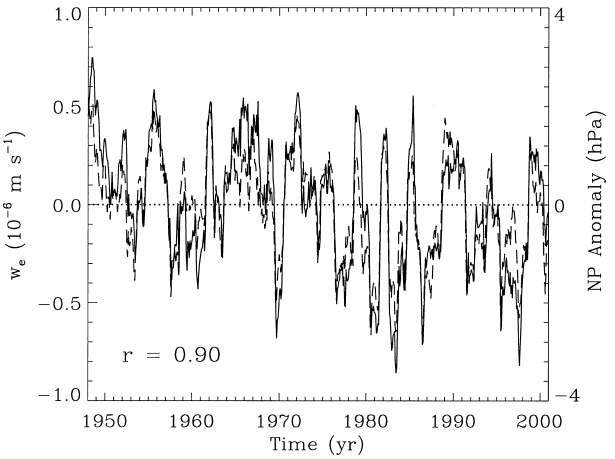

FIG. 3. The solid line gives the PC of the leading Ekman pumping velocity mode (Fig. 2a) with a 1-yr moving average filter applied. Plotted for comparison are similarly filtered sea level pressure anomalies of the North Pacific (NP) index (dashed line). Negative NP anomalies are associated with deepening of the Aleutian low. The correlation coefficient between the two time series is 0.90; for the unfiltered time series, $r = 0.83$.

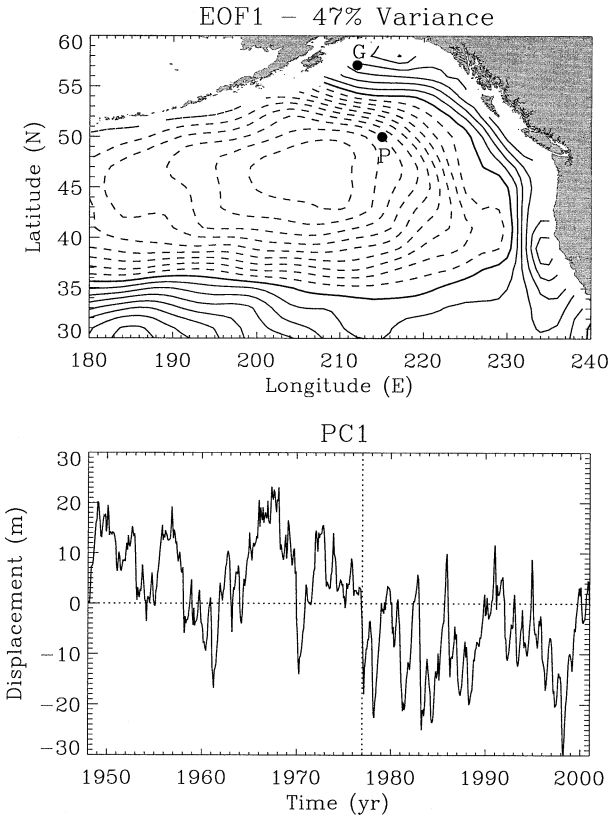

FIG. 4. The leading EOF and PC (referred to as EOF1 and PC1, respectively) of pycnocline depth variability from the reference case with $\lambda^{-1} = 1.5$ yr, and five Ekman pumping forcing EOFs ($M = 5$). The spatial pattern is contoured at intervals of 0.1 and the principal component is plotted in units of meters. Locations of Stations P and GAK11 are indicated in the upper panel. A dotted vertical line indicating 1977 is plotted with the PC to highlight the timing of the "regime shift."

unchanged if additional modes are included in the forcing. The additional modes increase the total variability in h, thereby reducing the fraction of variance associated with PC1. For example, the fractional variance represented by PC1 decreases from 48% to 40% as M is increased from 5 to 10.

The spatial structure of EOF1 is determined largely by the structure found in the first few Ekman pumping EOFs. The first forcing EOF (Fig. 2a) is clearly important and generally resembles the pattern of Fig. 4. However, the higher forcing modes, in particular modes 2 and 3, are required to produced an intensified response in the Gulf of Alaska. The superposition of these forcing modes produces the PDO-like spatial pattern with the central Pacific region anticorrelated with the Gulf of Alaska and near coastal regions. Miller et al. (1994) also found that the pattern of thermal variability in the upper ocean is set by the atmospheric forcing. The pattern of EOF1 is virtually insensitive to variations in λ^{-1}. Specifically, varying λ^{-1} through a range of values from 1 yr to ∞ (no damping) produces no appreciable change in the structure of EOF1.

While EOF1 is determined mainly by the structure of the forcing, PC1 shows considerable sensitivity to the damping timescale of the parameterized ocean dynamics. Figure 5 shows PC1 obtained with several different values of λ^{-1}. As the damping time scale is increased from 1 to 4 to 16 yr, the interannual variability is gradually suppressed and the response emphasizes the interdecadal variability. A transition or regime shift occurring during the late 1970s emerges as a robust aspect of the response for damping timescales of order 1–4 yr. The transition is delayed a few years as the decay timescale is increased from 4 to 16 yr. In the absence of any damping ($\lambda^{-1} = \infty$), the transition is delayed appreciably, occurring in the late-1980s. In this case, the response is dominated by a general positive trend from the beginning of the integration up to the mid-1970s, and then followed by a second long-term trend of opposite sign. These trends arise from integration of Ekman pumping velocities anomalies, which in the mean are negative over the central Pacific up to the mid-1970s and positive afterwards (e.g., Fig. 3).

The results shown in Fig. 5 suggest that the damping provided by internal ocean dynamics may have played an important role in controlling the timing of the late 1970s regime transition. This result may be understood in terms of the phase lag of the response, $\phi = \tan^{-1}(\omega/\lambda)$. This phase is advanced significantly at low frequencies relative to the undamped case in which $\phi = 90°$ for all ω. For example, with $\lambda^{-1} = 4$ yr and $\omega = 2\pi/50$ yr corresponding to the longest timescales in the record, the phase advance is 63°, or nearly 9 yr, relative to the undamped case.

EOF1 and PC1 given in Fig. 4 delineate an analog to the PDO in the response of the model to Ekman pumping. The spatial structure of EOF1 resembles the

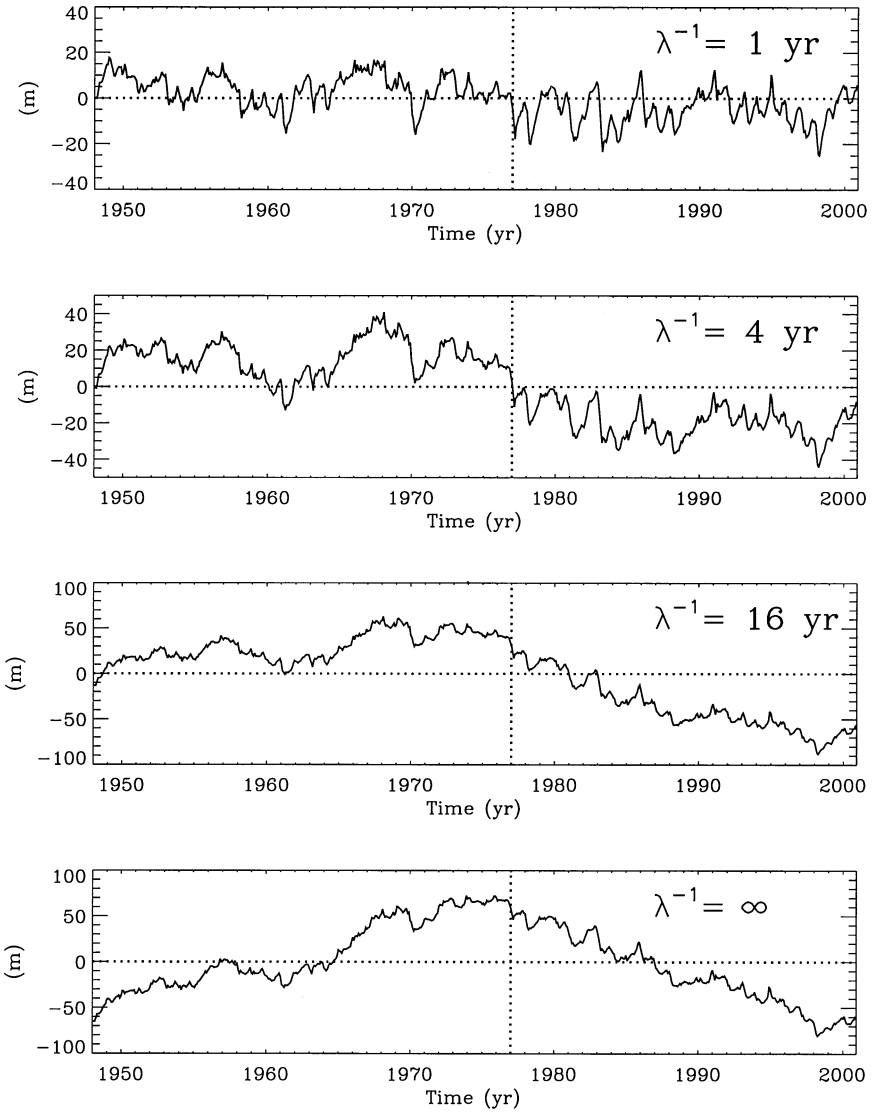

FIG. 5. PC1 time series obtained with various values of the damping timescale. In each case, $M = 5$. The bottom panel shows the principal component in the case of a purely passive oceanic response with no feedback.

canonical PDO pattern and PC1 is relatively well correlated with monthly values of the PDO index, as shown in Fig. 6. In the reference case, the correlation with the PDO index is 0.63. Table 1 gives the correlation coefficient between the PDO index and PC1 for cases with different values of λ^{-1} and M. The results show a relatively weak sensitivity to the damping timescale up to 4 yr. However, in the absence of any damping, the correlation with the PDO index is practically zero, underscoring the important dissipative function played by ocean dynamics in the temporal response to the forcing.

The entry in Table 1 with $M = 1$ shows that correspondence between PC1 and the PDO index is due largely to the first Ekman forcing mode (Fig. 2a); with only this single forcing mode, the correlation with the PDO index is 0.62. Inclusion of additional forcing modes has little effect on the correlation with the index but permits the PDO-like spatial pattern to emerge in the response. This result complements the earlier finding of Frankignoul and Hasselmann (1977) that a first-order autoregressive model represents accurately the lagged cross-correlation between the leading PCs of sea level pressure and SST over the North Pacific.

3. Variability at station P

Overall, the results of the previous section demonstrate that a mode of pycnocline variability bearing a spatial and temporal structure related to the PDO emerges readily in the response of a first-order autoregressive model driven by local Ekman pumping. We now consider the ability of this model to hindcast the pycnocline

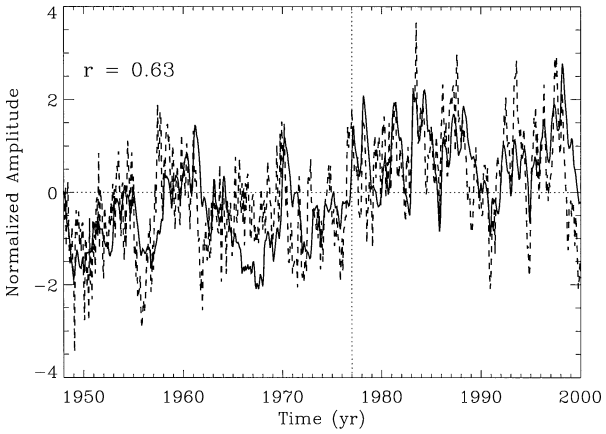

FIG. 6. Comparison between monthly values of the PDO index (dashed line) and the negative of PC1 (from Fig. 4, but sign reversed). The PDO index is based on an EOF analysis of SST over the extratropical North Pacific with globally averaged anomalies removed to separate any global warming signal. (The index is available online at ftp://ftp.atmos.washington.edu/mantua/pnw_impacts/INDICES/PDO.latest.)

depth variability observed at station P. It is worth noting that, in terms of the leading EOF, station P is located well within the covarying central Pacific region that is anticorrelated with the Gulf of Alaska and near-coastal eastern Pacific (Fig. 4). This is in contrast to analyses of SST (e.g., Zhang et al. 1997) that show station P to the east of the zero contour, within the covarying near-coastal region.

Station P provides a unique long time series to compare the model pycnocline depth variability directly with observations. These consist of bottle cast and CTD data that are used to examine low-frequency variability of the subsurface density field. Freeland et al. (1997) constructed a least squares fit of density observations to a two-layer model of the density structure. The two-layer representation is appropriate for wintertime data and it tracks accurately the core of the main pycnocline.[2] An average of the fitted wintertime (January–April) values for each year was formed to obtain a time series of the depth of the main pycnocline for the period 1957–94. (Results are little changed if the wintertime mean is redefined in terms of December–April observations.) The time series has been augmented by more recent observations from 1995 to 1999. In addition, a data point for 1991 that had originally been inadvertently omitted is now included. One data point (1994) has been removed because it was from a station 200 km away, along line P. The resulting yearly time series covers the period 1957–99 with gaps in 1985, 1988, 1990, and 1994.

The number of data values available to determine the yearly means is variable. Generally, there are many more observations over the earlier period, 1957–81, when station P was occupied on a continuous basis by a weather ship. For those years in which five or more observations were available to compute the mean, we have also determined the standard deviation about the mean. Higher-frequency processes such as mesoscale eddies and baroclinic tides may contribute to some of the variability about the computed means. For example, Thomson and Tabata (1982) observed rms displacements of 2–4 m in the main pycnocline within the semidiurnal frequency band.

TABLE 1. Correlation coefficient r between PC1 and the PDO index for various values of the damping timescale λ^{-1} and the number of Ekman pumping forcing modes M.

λ^{-1} (yr)	M	r
1	5	0.65
1	10	0.66
1.5	1	0.62
1.5	5	0.63
1.5	10	0.63
1.5	20	0.62
2	5	0.61
2	10	0.61
4	5	0.56
4	10	0.56
∞	5	0.06
∞	10	0.06

Figure 7 shows the comparison between annual mean values of the pynocline displacement from the model and the observed displacement anomalies at station P. The model response is from the reference case ($\lambda^{-1} = 1.5$ yr, $M = 5$) evaluated at the grid point corresponding to the location of station P. For direct comparison with the observations, gaps corresponding to the 4 years of missing data have been introduced into the modeled time series. The result clearly gives a good account of the observations over the entire record with a correlation coefficient, $r = 0.77$. The modeled time series is nearly always within a standard deviation of the data. At station P, the main pycnocline has exhibited substantial depth variations with a maximum range of approximately ± 25 m about a long-term mean depth of ~ 120 m. Anomalies have tended to be generally negative (deeper pycnocline) prior to late 1970s and positive over following two decades, hence the net shoaling trend detected by Freeland et al. (1997). The results shown here demonstrate that these variations are accounted for by local Ekman pumping.

The sensitivity of the model response at station P to variations in λ^{-1} and the number of forcing modes, M, is summarized in Table 2. The results are compared on the basis of the correlation coefficient, r, and the ratio of the variance of the model anomalies to that of the observations, $\gamma^2 = \sigma_m^2/\sigma_o^2$, where $\sigma_o^2 = 127.8\ \mathrm{m}^2$. Also defined is a related measure of "skill," $S = 1 - \langle (h - h_o)^2 \rangle / \langle h_o^2 \rangle = 2r\gamma - \gamma^2$, where the angle brackets denote

[2] Although Freeland et al. (1997) refer to the fitted depths as "mixed-layer depths," they correspond more closely to the depth of the core of the main pycnocline, as their Fig. 1c demonstrates.

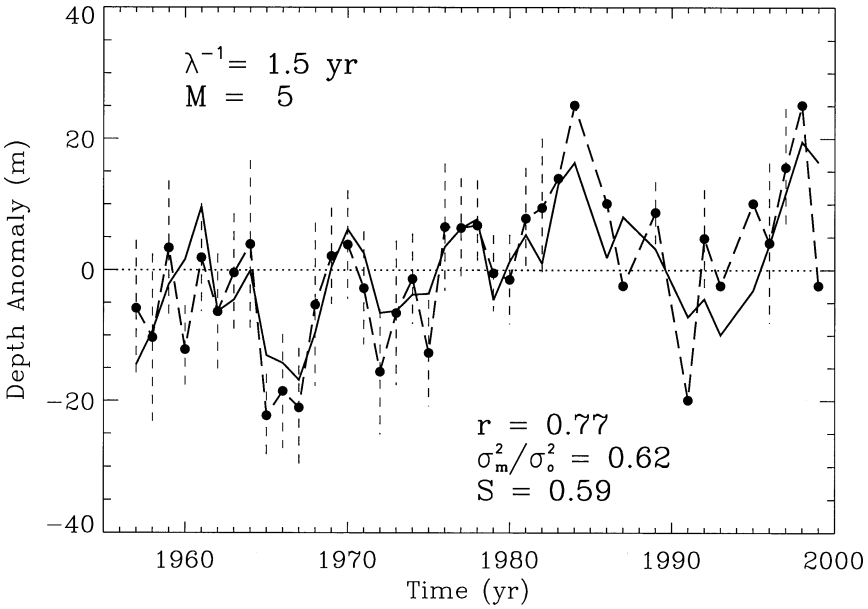

FIG. 7. Comparison of mean wintertime pycnocline depth anomalies observed at station P (dashed line) with annual mean anomalies predicted from the reference case with the model (λ^{-1} = 1.5 yr, M = 5). For years with at least five observations, ±1 standard deviation about the observed mean is indicated by the vertical dashed lines.

a time averaging, and h_o are the observed depth anomalies.

The results of Table 2 show that the correlation coefficient is only weakly sensitive to the parameters over the tested range, decreasing gradually as the decay timescale is increased beyond 1.5 yr. On the other hand, with a shorter decay timescale the variability is somewhat weaker than observed. If the model is forced with only the leading Ekman pumping velocity mode (M = 1 in Table 2), a high correlation (r = 0.78) is obtained with the station P data. However, the magnitude of the variability obtained from forcing with this single mode is small compared to observations; evidently the higher modes contribute significantly. The parameters used in the reference case appear to be close to optimal. However, comparable results are obtained with a damping timescale varying between 1 and 2 yr and with 5–10 forcing modes. The line in Table 2 with the entry ''no filtering'' gives the result when the EOF truncation of the Ekman pumping velocity is omitted, equivalent to including all the modes in the forcing. In comparison to the reference case, the correlation coefficient is somewhat lower and the index of skill is reduced by a factor of nearly 2.

TABLE 2. Comparison between hindcast pycnocline depth anomalies at station P and observed anomalies. The correlation coefficient r, ratio of variances σ_m^2/σ_o^2, and skill S are given for various values of λ^{-1} and M. The line with the entry ''no filtering'' is for a case in which EOF filtering of the Ekman pumping velocity fields was omitted.

λ^{-1} (yr)	M	r	σ_m^2/σ_o^2	S
1	5	0.77	0.39	0.57
1	10	0.75	0.44	0.55
1.5	1	0.78	0.20	0.49
1.5	5	0.77	0.62	0.59
1.5	10	0.74	0.70	0.54
1.5	20	0.71	0.95	0.44
1.5	No filtering	0.64	0.86	0.32
2	5	0.75	0.83	0.54
2	10	0.73	0.92	0.47
3	5	0.73	1.22	0.40
3	10	0.70	1.33	0.29

The influence of the late-1970s regime transition is evident in the station P record and much of the model variability shown in Fig. 7 is associated with (EOF1, PC1), the PDO analog of Fig. 4. In particular, the shoaling of the pycnocline at station P observed after 1977 is consistent with Fig. 4. Accordingly, the correlation is −0.78 between the anomalies observed at station P and annually averaged values of PC1. Overland et al. (1999) examine density profiles at station GAK11 in the Gulf of Alaska (57.1°N, 212°E; Fig. 4) and showed a deepening of the main pycnocline between the mid-1970s and mid-1980s. These changes, along with the dynamic height variability discussed by Lagerloef (1995), are also consistent with the pattern of Fig. 4, which indicates a long-lived deepening of the pycnocline over the central Gulf of Alaska after 1977.

4. Conclusions

This study has examined the low-frequency variability arising from Ekman pumping at station P and over the northeast Pacific in terms of the stochastic climate model

of Hasselmann (1976). In particular, we have considered the extent that the observed pycnocline depth anomalies reported by Freeland et al. (1997) could be explained in terms of this simple autoregressive model. We also examined the contribution that a PDO mode of variability may have made to the changes observed at station P.

The principal result is that a large fraction of the low-frequency variability in the depth of the pycnocline at station P can be explained in terms of a first-order autoregressive process driven by local Ekman pumping. In particular, the shoaling of the pycnocline noted by Freeland et al. (1997) over the period 1957–94 occurred as an integrated response to the local wind forcing. This conclusion is consistent with the results of Lagerloef (1995) regarding low-frequency dynamic height variability in the Gulf of Alaska.

An analog to the PDO emerges as the leading EOF of the autoregressive model over the northeast Pacific. This mode apparently has had an important influence on the variability at station P, largely accounting for the shoaling of the pycnocline. With respect to pycnocline depth variability, station P lies within the covarying central Pacific region of the PDO mode, rather than within the near-coastal region, as indicated in SST analyses.

Our results suggest that dissipative aspects of ocean dynamics are important to the response over the northeast Pacific. While a damping timescale of 1–2 yr is appropriate, the nature of these dissipative processes is unresolved. Possible mechanisms may involve turbulent mixing and entrainment/detrainment, lateral eddy fluxes, and gyre-scale advection. On the other hand, it is remarkable that the observations of low-frequency, baroclinic variability at station P can be accounted for without invoking Rossby wave or Sverdrup dynamics. One possible reason is that at subpolar latitudes the timescale of decay may be sufficiently short in comparison with the timescale of propagation that Rossby waves are attenuated while still in proximity of the eastern boundary. For example, based on the theoretical long wave speed for the subarctic Pacific ($\sim$0.5 cm s^{-1}), a wave originating from the coast would require nearly 8 years to reach station P. The possible influence of baroclinic Rossby waves on low-frequency variability in the northeast Pacific will be explored in future work.

Acknowledgments. The NCEP reanalysis data were provided by the NOAA–CIRES Climate Diagnostics Center, Boulder, Colorado, from their Web site, http://www.cdc.noaa.gov/. Howard Freeland graciously provided results from the two-layer fit to the station P data. Rick Thomson, Howard Freeland, and Art Miller offered useful comments on the manuscript.

REFERENCES

Chave, A. D., D. S. Luther, and J. H. Filloux, 1991: Variability of the wind stress curl over the North Pacific: Implications for the oceanic response. *J. Geophys. Res.,* **96,** 18 361–18 379.

Deser, C., M. A. Alexander, and M. S. Timlin, 1996: Upper-ocean thermal variations in the North Pacific during 1970–1991. *J. Climate,* **9,** 1840–1855.

Frankignoul, C., and K. Hasselmann, 1977: Stochastic climate models. Part II: Application to sea-surface temperature anomalies and thermocline variability. *Tellus,* **29,** 289–305.

——, P. Müller, and E. Zorita, 1997: A simple model of the decadal response of the ocean to stochastic wind forcing. *J. Phys. Oceanogr.,* **27,** 1533–1546.

Freeland, H. J., K. Denman, C. S. Wong, F. Whitney, and R. Jacques, 1997: Evidence of change in the winter mixed layer in the northeast Pacific Ocean. *Deep-Sea Res.,* **44,** 2117–2129.

Hasselmann, K., 1976: Stochastic climate models. Part I: Theory. *Tellus,* **28,** 473–485.

Lagerloef, G. S. E., 1995: Interdecadal variations in the Alaska gyre. *J. Phys. Oceanogr.,* **25,** 2242–2258.

——, R. Lucas, R. A. Weller, and S. P. Anderson, 1998: Pacific warm pool surface temperature regulation during TOGA COARE: Upper ocean feedback. *J. Climate,* **11,** 2297–2309.

Latif, M., and T. P. Barnett, 1994: Causes of decadal climate variability over the North Pacific and North America. *Science,* **266,** 634–637.

Mantua, N. J., S. R. Hare, Y. Zhang, J. M. Wallace, and R. C. Francis, 1997: A Pacific interdecadal climate oscillation with impacts on salmon production. *Bull. Amer. Meteor. Soc.,* **78,** 1069–1079.

Miller, A. J., and N. Schneider, 2000: Interdecadal climate regime dynamics in the North Pacific Ocean: Theories, observations and ecosystem impacts. *Progress in Oceanography,* Vol. 47, Pergamon, 355–397.

——, D. R. Cayan, T. P. Barnett, N. E. Graham, and J. M. Oberhuber, 1994: Interdecadal variability of the Pacific Ocean: Model response to observed heat flux and wind stress anomalies. *Climate Dyn.,* **9,** 287–302.

——, ——, and W. B. White, 1998: A westward-intensified decadal change in the North Pacific thermocline and gyre-scale circulation. *J. Climate,* **11,** 3112–3127.

Müller, P., and C. Frankignoul, 1981: Direct atmospheric forcing of geostrophic eddies. *J. Phys. Oceanogr.,* **11,** 287–308.

North, G. R., T. L. Bell, R. F. Cahalan, and F. J. Moeng, 1982: Sampling errors in the estimation of empirical orthogonal functions. *Mon. Wea. Rev.,* **110,** 699–706.

Overland, J. E., S. Salo, and J. M. Adams, 1999: Salinity signature of the Pacific Decadal Oscillation. *Geophys. Res. Lett.,* **26,** 1337–1340.

Preisendorfer, R. W., 1988: *Principal Component Analysis in Meteorology and Oceanography.* Developments in Atmospheric Science, Vol. 17, C. D. Mobley, Ed. Elsevier, 425 pp.

Qui, B., 2002: Large-scale variability in the midlatitude subtropical and subpolar North Pacific Ocean: Observations and causes. *J. Phys. Oceanogr.,* **32,** 353–375.

Reinecker, M. M., and L. L. Ehret, 1988: Wind stress curl variability over the North Pacific from the Comprehensive Ocean–Atmosphere Data Set. *J. Geophys. Res.,* **93,** 5069–5077.

Thomson, R. E., and S. Tabata, 1982: Baroclinic oscillations of tidal frequency at Ocean Weather Station P. *Atmos.–Ocean,* **20,** 242–257.

Tourre, Y. M., M. Kushnir, and W. B. White, 1999: Evolution of interdecadal variability in sea level pressure, sea surface temperature, and upper ocean temperature over the Pacific Ocean. *J. Phys. Oceanogr.,* **29,** 1528–1541.

——, ——, and ——, 2001: Patterns of coherent decadal and interdecadal climate signals in the Pacific basin during the 20th century. *Geophys. Res. Lett.,* **28,** 2069–2072.

Trenberth, K. E., and J. W. Hurrell, 1994: Decadal atmosphere–ocean variations in the Pacific. *Climate Dyn.,* **9,** 303–319.

von Storch, H., and F. W. Zwiers, 1999: *Statistical Analysis in Climate Research.* Cambridge University Press, 484 pp.

White, W. B., and D. R. Cayan, 1998: Quasi-periodicity and global symmetries in interdecadal upper ocean temperature variability. *J. Geophys. Res.,* **103,** 21 335–21 354.

Zhang, Y., J. M. Wallace, and D. S. Battisti, 1997: ENSO-like interdecadal variability: 1900–93. *J. Climate,* **10,** 1004–1020.